arXiv:1209.0239v1 [cond-mat.str-el] 3 Sep 2012

Dynamical Jahn-Teller Effect in Spin-Orbital Coupled System

Joji Nasu and Sumio Ishihara
Department of Physics, Tohoku University, Sendai 980-8578, Japan
(Dated: September 4, 2012)

Dynamical Jahn-Teller (DJT) effect in spin-orbital coupled system on a honeycomb lattice is examined, motivated from recently observed spin-liquid behavior in $Ba_3CuSb_2O_9$. Effective vibronic Hamiltonian, where the superexchange interaction and the DJT effect are taken into account, is derived. We find that the DJT effect induces a spin-orbital resonant state where local spin-singlet states and parallel orbital configurations are entangled with each other. This spin-orbital resonant state is realized in between an orbital ordered state, where spin-singlet pairs are localized, and an antiferromagnetic ordered state. Based on the theoretical results, a possible scenario for $Ba_3CuSb_2O_9$ is proposed.

PACS numbers: 75.25.Dk, 75.30.Et,75.47.Lx

No signs for long-range magnetic ordering down to the low temperatures, terms the quantum spin-liquid (QSL) state, are one of the fascinating states of matter in modern condensed matter physics [1]. A number of efforts have been done to realize the QSL states theoretically and experimentally. One prototypical example is the well known one-dimensional antiferromagnetic spin chains in which large quantum fluctuation destroys the long-range spin order even at zero temperature and realizes a spin-singlet state without any symmetry breakings. Another candidate for the QSL states has been searched for a long time in frustrated magnets. An organic salt κ-(BEDT-TTF)$_2$Cu$_2$(CN)$_3$ with a triangular lattice [2] and an inorganic herbertsmithite $ZnCu_3(OH)_6Cl_2$ with a Kagomé lattice [3] are some examples. Several theoretical scenarios for realization of the QSL, such as Z_2-spin liquid [4], spin-nematic state [5], spinon-deconfinement [6] and so on, have been proposed so far.

A transition-metal oxide of our present interest is a new candidate of the QSL state, $Ba_3CuSb_2O_9$, in which $S = 1/2$ spins in Cu^{2+} ions are responsible for the magnetism [7, 8]. There are no signs of magnetic orderings down to a few hundred mK, in spite of the effective exchange interactions of 30-50K. Temperature dependences of the magnetic susceptibility and the electronic specific heat are decomposed into the gapped component and the low-energy component, which is attributed to the so-called orphan spins [8]. It was believed that the QSL behavior originates from the magnetic frustration in a Cu^{2+} triangular lattice. Recent detailed crystal-structural analyses reveal that Cu ions are regularly replaced by Sb ions, and form a short-range honeycomb lattice [8]. One characteristic in the present QSL system is that there is the orbital degree of freedom; two-fold orbital degeneracy in Cu^{2+} is suggested by the three-fold rotational symmetry around a Cu^{2+}. Almost isotropic g-factors observed in the electron-spin resonance (ESR) provide a possibility of no static long-range orbital orders and novel roles of orbital on the QSL.

In this Letter, motivated from the recent experiments in $Ba_3CuSb_2O_9$, we examine a possibility of the QSL state in a honeycomb-lattice spin-orbital system. Beyond the previous theories for QSL in quantum magnets with the orbital degree of freedom [9–13], the present theory focuses on the dynamical Jahn-Teller (DJT) effect, which brings about a quantum tunneling between stable orbital-lattice states. This is feasible in the crystal lattice of $Ba_3CuSb_2O_9$ where O_6 octahedra surrounding Cu^{2+} are separated with each other, unlike the perovskite lattice where nearest-neighboring (NN) two octahedra share an O^{2-}. The spin-orbital superexchange (SE) interactions between the separated NN Cu^{2+} are comparable with the vibronic interactions, and a new state of matter is expected as a result of the competition between the on-site Jahn-Teller (JT) and inter-site SE interactions. We derive the low-energy electron-lattice coupled model where the SE interaction, the JT effect, and the lattice dynamics are taken into account. It is discovered that a spin-orbital resonant state, where the two degrees of freedom are entangled with each other, is induced by the DJT effect. We examine connections of the present quantum resonant state to a spin ordered state and an orbital ordered state, and provide a possible scenario for $Ba_3CuSb_2O_9$.

In a CuO_6 octahedral cage with the C_{3v} symmetry, one hole in Cu^{2+} occupies doubly degenerate E orbitals, which are approximately $3d_{3z^2-r^2}$ and $3d_{x^2-y^2}$. We set up a model where the CuO_6 octahedra are arranged on a honeycomb lattice [see Fig. 1(a)] by taking into account the recent x-ray scattering experiments [8]. The starting Hamiltonian consists of the electronic term $\mathcal{H}_{dp}$ and the electron-lattice interaction term $\mathcal{H}_{e\text{-}l}$. The electronic term is the dp-type Hamiltonian where the degenerate $3d_{3z^2-r^2}$ and $3d_{x^2-y^2}$ orbitals in Cu^{2+} and the three $2p$ orbitals in O^{2-} are introduced. The electron transfers between the Cu and O sites (t_{dp}), those between the different O sites (t_{pp}), and the Coulomb and exchange interactions in Cu and O ions are taken into account. Details are given in Supplemental Material (SM) [14]. As for the electron-lattice interaction term, the two vibrational modes for an O_6 cage with the E_g symmetry, Q_u and Q_v, couple with the $3d_{3z^2-r^2}$ and $3d_{x^2-y^2}$ orbitals. This is given as $\mathcal{H}_{e\text{-}l} = \sum_i [-(2M)^{-1}\left(\partial^2/(\partial Q_{ui}^2) + \partial^2/(\partial Q_{vi}^2)\right) + M\omega^2\rho_i^2/2 + 2A(T_i^x Q_{vi} + T_i^z Q_{ui}) + B(Q_{ui}^3 - 3Q_{vi}^2 Q_{ui})]$, here $\rho_i = \sqrt{Q_{ui}^2 + Q_{vi}^2}$ is an amplitude of the lattice distortion, and $\boldsymbol{T}_i$ is the pseudo-spin (PS) operator for the doubly-degenerate orbitals with an amplitude $1/2$. The first and second terms describe the harmonic vibrations with frequency ω and ionic mass M. The third term describes the JT coupling

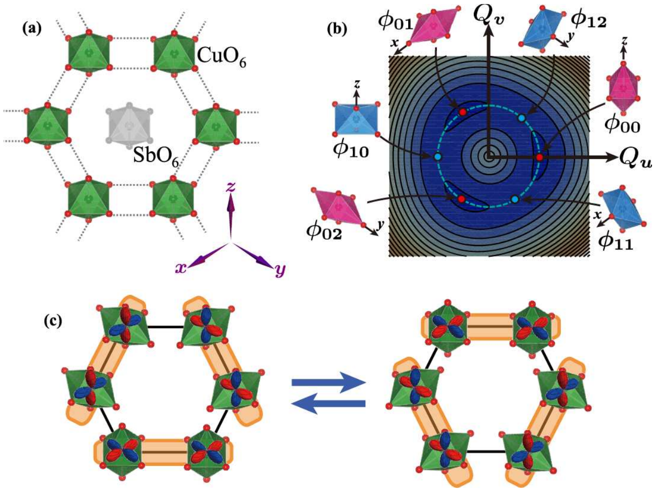

FIG. 1: (color online). (a) A honeycomb lattice structure for Ba$_3$CuSb$_2$O$_9$. The axes of coordinates, x, y, z, are taken to be along the NN Cu-O bond directions in an octahedron. (b) A contour map of the lower AP surface $U^{(-)}$ on the Q_u-Q_v plane. A blue broken line shows a circle for $\rho = \rho_0$. Schematic O$_6$ distortions at the potential minima and maxima are also shown. (c) A schematic picture for the spin-orbital resonance state. Shaded bonds represent the spin-singlet and parallel-orbital bonds.

with a coupling constant $A (> 0)$, and the last term represents the anharmonic lattice potential, where B is negative in most of Cu^{2+}.

Here, we compare several energy scales. In the electronic part, the on-site Coulomb interaction at Cu^{2+} is U_d ~5-10eV which is much larger than the Cu-O and O-O hybridizations $t_{pd} \sim t_{pp} \sim$ 1eV. The SE interaction is J ~1-10meV, which is smaller than that in the high-T_c cuprates due to a large distance between the NN Cu sites. As well known in the $E \otimes e$ JT problem [15], two adiabatic potentials (APs) are given by $U^{(\pm)} = M\omega^2\rho^2 \pm A\rho + B\cos 3\theta$ where $\theta = \tan^{-1}(Q_v/Q_u)$. The largest energy scale in the vibronic part is provided by the JT energy $E_{\rm JT} [= A^2/(2M\omega^2) = M\omega^2\rho_0^2/2]$ which is of the order of 0.1-1eV. We introduce $\rho_0 = A/(M\omega^2)$ at which the lower AP, $U^{(-)}$, takes its minima in the case of $B = 0$. The anharmonic-potential energy $E_{\rm AH} (= |B|\rho_0^3)$, the lattice kinetic energy for the azimuthal rotation on the Q_u-Q_v plane $E_{\rm rot} [= \omega^2/E_{\rm JT} = 2/(M\rho_0^2)]$, and the zero-point vibrational energy $E_{\rm zero} (= \omega/2)$ are of the orders of 1-10meV, 1-10meV and 10-100meV, respectively. From these estimations, we draw a following picture for the low-energy electronic and vibrational states up to about 10meV: the local vibronic system is confined on the lower AP surface, and a vibronic state dynamically tunnels during the three potential minima caused by the anharmonic potential [see Fig. 1(b)]. This local vibronic state competes with the spin-orbital state stabilized by the inter-site SE interactions.

Based on this picture, the low-energy effective model is derived. The SE interactions between the NN Cu ions are obtained by the perturbational calculations. The effective Hamiltonian is given by

$$\mathcal{H}_{\rm exch} = \sum_{\langle ij \rangle_l} \Big[J_{ss} \boldsymbol{S}_i \cdot \boldsymbol{S}_j + J_{\tau\tau} \tau_i^l \tau_j^l + J_{\bar{\tau}\bar{\tau}} \bar{\tau}_i^l \bar{\tau}_j^l + J_{yy} T_i^y T_j^y + J_{ss\tau} \boldsymbol{S}_i \cdot \boldsymbol{S}_j (\tau_i^l + \tau_j^l) + J_{ss\tau\tau} \boldsymbol{S}_i \cdot \boldsymbol{S}_j \tau_i^l \tau_j^l + J_{ss\bar{\tau}\bar{\tau}} \boldsymbol{S}_i \cdot \boldsymbol{S}_j \bar{\tau}_i^l \bar{\tau}_j^l + J_{ssyy} \boldsymbol{S}_i \cdot \boldsymbol{S}_j T_i^y T_j^y \Big], \tag{1}$$

where $\boldsymbol{S}_i$ is the spin operator with an amplitude 1/2, and $\langle ij \rangle_l$ is the NN Cu sites along one of the bond directions $l (= x, y, z)$ defined in Fig. 1(a) [16]. For convenience, we introduce $\tau_i^l = \cos(2\pi n_l/3) T_i^z - \sin(2\pi n_l/3) T_i^x$ and $\bar{\tau}_i^l = \cos(2\pi n_l/3) T_i^x + \sin(2\pi n_l/3) T_i^z$ with $(n_z, n_x, n_y) = (0, 1, 2)$. The eigen state of τ^l with the eigen value +1/2 (-1/2) corresponds to the state where $d_{3l^2-r^2}$ ($d_{m^2-n^2}$) orbital is occupied by a hole and (l, m, n) are the cyclic permutations of the Cartesian coordinates. Detailed derivation is given in SM [14]. For the two NN Cu sites, we find that this exchange Hamiltonian favors an antiferromagnetic (AFM) and ferro-type orbital configuration in a wide parameter region which includes a realistic parameter set for Ba$_3$CuSb$_2$O$_9$ [14, 17]. This is due to the Cu-O-O-Cu exchange paths, and is in contrast to the conventional ferromagnetic and staggered-type orbital configuration realized in the corner-sheared two octahedra [18].

As for the vibrational term, we focus on the rotational mode on the lower AP surface where an angle $\theta \equiv \tan^{-1}(Q_v/Q_u)$ is varied with a fixed amplitude at $\rho = \rho_0$. The rotational-mode Hamiltonian for a single octahedron is given by $\mathcal{H}_{\rm rot} = -(2M\rho_0^2)^{-1}\partial^2/(\partial\theta^2) + B\rho_0^3 \cos 3\theta$ [15, 19]. The second term takes its minima (maxima) at angles $\theta_{\mu\nu} = \pi\mu + 2\pi\nu/3$ with $\nu = (0, 1, 2)$ for $\mu = 0$ ($\mu = 1$). The lowest-six eigen states for $\mathcal{H}_{\rm rot}$ are transformed into the Wannier-type wave functions $\phi_{\mu\nu}(\theta)$ which are almost localized around $\theta_{\mu\nu}$ [see Fig. 1(b)]. We adopt, as the basis set, the six vibronic wave functions $\Phi_{\mu\nu}(\boldsymbol{r};\theta) = \psi(\boldsymbol{r};\theta)\phi_{\mu\nu}(\theta)$, where $\psi(\boldsymbol{r};\theta) = \psi_{x^2-y^2}(\boldsymbol{r})\cos(\theta/2) - \psi_{3z^2-r^2}(\boldsymbol{r})\sin(\theta/2)$ is the wave function for a hole. Then, the low-energy vibronic Hamiltonian is represented by a simple form;

$$\mathcal{H}_{\rm JT} = \frac{1}{2} \sum_i \sum_{l=0}^{2} \sigma_i^z \otimes \left(J_{\rm DJT} D_i^l - \frac{J_{\rm AH}}{2} D_i^{l2} \right), \tag{2}$$

where σ_i^z is the z component of the Pauli matrices and is defined for the index μ=0 and 1. We introduce 3×3 matrices $(D^l)_{\nu\nu'} = |\varepsilon_{l\nu\nu'}|$, where $\varepsilon_{l\nu\nu'}$ are the Levi-Civita completely antisymmetric tensors, for the index ν. The first and second terms represent the vibronic motion and the anharmonic lattice potential, respectively, and $J_{\rm DJT}$ and $J_{\rm AH}$ are the constants of the order of $\omega^2/E_{\rm JT}$ and $|B|\rho_0^3$, respectively. The condition $J_{\rm DJT}/J_{\rm AH} < 1/2$ is required to reproduce the eigen states of $\mathcal{H}_{\rm rot}$, but we regards $J_{\rm DJT}/J_{\rm AH} (\equiv j_D)$ as a free parameter, for convenience. The lowest energy state for $\mathcal{H}_{\rm JT}$ is a doublet, which corresponds to the clockwise and counter-clockwise rotations described by the nodeless wave functions in the θ space. The detailed derivation of $\mathcal{H}_{\rm JT}$ is

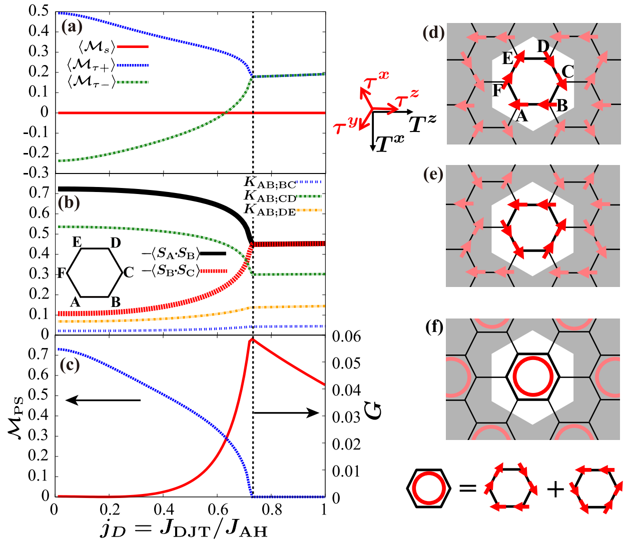

FIG. 2: (color online). (a) Staggered spin moment $\mathcal{M}_s$, and two PS moments $\mathcal{M}_{\tau+}$ and $\mathcal{M}_{\tau-}$. (b) Spin-correlations $\langle \boldsymbol{S}_\mathrm{A} \cdot \boldsymbol{S}_\mathrm{B}\rangle$ and $\langle \boldsymbol{S}_\mathrm{B} \cdot \boldsymbol{S}_\mathrm{C}\rangle$ (bold lines), and spin-dimer correlations $K_{\mathrm{AB;BC}}$, $K_{\mathrm{AB;CD}}$ and $K_{\mathrm{AB;DE}}$ (thin lines). The inset shows a 6-site cluster. We obtain $\langle \boldsymbol{S}_\mathrm{A} \cdot \boldsymbol{S}_\mathrm{B}\rangle = \langle \boldsymbol{S}_\mathrm{C} \cdot \boldsymbol{S}_\mathrm{D}\rangle = \langle \boldsymbol{S}_\mathrm{E} \cdot \boldsymbol{S}_\mathrm{F}\rangle$ and $\langle \boldsymbol{S}_\mathrm{B} \cdot \boldsymbol{S}_\mathrm{C}\rangle = \langle \boldsymbol{S}_\mathrm{D} \cdot \boldsymbol{S}_\mathrm{E}\rangle = \langle \boldsymbol{S}_\mathrm{F} \cdot \boldsymbol{S}_\mathrm{A}\rangle$. (c) Spin-orbital correlation function G, and the three-fold orbital order parameter $\mathcal{M}_{\mathrm{PS}}$. The broken line indicates j_{Dc}. (d) (e) Two kinds of the three-fold orbital ordered states. (f) A schematic spin-orbital resonance state. Arrows represent the orbital PSs.

given in SM [14]. Finally, the exchange and vibronic terms are taken together as the low-energy effective Hamiltonian; $\mathcal{H}_{\mathrm{eff}} = \mathcal{H}_{\mathrm{exch}} + \mathcal{H}_{\mathrm{JT}}$.

This Hamiltonian is analyzed by the exact diagonalization (ED) method combined with the mean-field (MF) approximation, and the quantum Monte-Carlo simulation (QMC) with the MF approximation, termed the ED+MF and the QMC+MF methods, respectively. We introduce mainly the results by the ED+MF method. The mean-field type decouplings are introduced in the exchange interactions which act on the edge sites of clusters. The Hamiltonian for a 6-site cluster under the MFs is diagonalized by the Lanczos algorithm, and the MFs are determined consistently with the states inside the cluster. The adopted parameter values are $J_{ss}/J_{\mathrm{AH}} = 0.15$ and given in Ref. [14]. We find that the obtained results do not depend qualitatively on the parameter J_{ss}/J_{AH} between 0.075 and 1.5. The exchange Hamiltonian $\mathcal{H}_{\mathrm{exch}}$ is also analyzed by the MF approximation and by the ED method as supplementary calculations.

Spin and orbital structures are examined as functions of amplitude of the DJT effect, i.e. $j_D = J_{\mathrm{DJT}}/J_{\mathrm{AH}}$. We introduce the staggered spin moment $\mathcal{M}_s = \frac{1}{6}\sum_i (-1)^i S_i^z$, and the two PS moments defined by $\mathcal{M}_{\tau+} = -\frac{1}{6}(\tau_\mathrm{A}^z + \tau_\mathrm{B}^z + \tau_\mathrm{C}^x + \tau_\mathrm{D}^x + \tau_\mathrm{E}^y + \tau_\mathrm{F}^y)$ and $\mathcal{M}_{\tau-} = -\frac{1}{6}(\tau_\mathrm{A}^x + \tau_\mathrm{B}^y + \tau_\mathrm{C}^y + \tau_\mathrm{D}^z + \tau_\mathrm{E}^z + \tau_\mathrm{F}^x)$ where subscripts A-F indicate sites in the cluster [see the inset of Fig. 2(b)]. We note that $\mathcal{M}_{\tau+}$ and $\mathcal{M}_{\tau-}$ take their maxima of 0.5 in the three-fold orbital ordered states shown in Figs. 2(d) and (e), respectively. A difference between the two, $\mathcal{M}_{\mathrm{PS}} \equiv \langle \mathcal{M}_{\tau+} - \mathcal{M}_{\tau-}\rangle$, is regarded as an order parameter for the three-fold orbital ordered state. The numerical results are plotted in Fig. 2(a). There is a critical value of j_D, termed $j_{Dc}(= 0.75)$. For $j_D \ll j_{Dc}$, $\mathcal{M}_{\tau+} = 0.5$ and $\mathcal{M}_{\tau-} = -0.25$, implying a symmetry breaking, i.e. the three-fold orbital ordered state shown in Fig. 2(d). This orbital order is also suggested by the analyses of $\mathcal{H}_{\mathrm{exch}}$. With increasing j_D, absolute values of both the two PS moments are reduced. These reductions are reproduced by the QMC+MF method. In a region of $j_D > j_{Dc}$, $\langle\mathcal{M}_{\tau+}\rangle = \langle\mathcal{M}_{\tau-}\rangle$ which is interpreted as a superposition of the two PS configurations shown in Fig. 2(f).

As for the spin sector, a finite staggered spin moment [see Fig. 2(a)], as well as a finite local spin moment $\langle S_i^z\rangle$ at each site, do not appear in a whole parameter region of j_D. As shown in Fig. 2(b), there are the two inequivalent NN spin correlations $\langle \boldsymbol{S}_i \cdot \boldsymbol{S}_j\rangle$ for $j_D < j_{Dc}$: large values are shown in the bonds where the PSs are parallel with each other. On the other hand, for $j_D > j_{Dc}$, $\langle \boldsymbol{S}_i \cdot \boldsymbol{S}_j\rangle$ for all bonds are equivalent. Spin-dimer correlations defined by $K_{ij;kl} = \langle(\boldsymbol{S}_i \cdot \boldsymbol{S}_j)(\boldsymbol{S}_k \cdot \boldsymbol{S}_l)\rangle$ provide information for the bond correlation. We plot $K_{\mathrm{AB;BC}}$, $K_{\mathrm{AB;CD}}$ and $K_{\mathrm{AB;DE}}$ which represent the bond-correlation functions for the NN bonds, the 2nd-NN bonds, and the 3rd-NN bonds, respectively. In a whole parameter region, the 2nd-NN bond correlation function, $K_{\mathrm{AB;CD}}$, is the largest. It is also shown that $K_{\mathrm{AB;CD}}$ in $j_D < j_{Dc}$ is larger than that in $j_D > j_{Dc}$. The results in $j_D < j_{Dc}$ are interpreted as a valence-bond solid state, where spin-singlet pairs are localized at the bonds, in which the NN PSs are parallel with each other. This spin and orbital structure is also confirmed in the analysis by the QMC+MF method. Above j_{Dc}, this state is changed into a superposition of the PS configurations, where the spin-singlet dimers are not localized in specific bonds, suggested by a reduction of $K_{\mathrm{AB;CD}}$ and enhancements of $K_{\mathrm{AB;BC}}$ and $K_{\mathrm{AB;DE}}$.

We expect from these data that, above j_{Dc}, the local spin singlet and the parallel PS configuration are strongly entangled quantum mechanically. This is confirmed by the spin-orbital correlation function defined by $G = [\frac{1}{6}\sum_{\langle ij\rangle_l} G_{ij}^l]^2$ with $G_{ij}^l = 16[\langle(\boldsymbol{S}_i \cdot \boldsymbol{S}_j)(\tau_i^l \tau_j^l)\rangle - \langle \boldsymbol{S}_i \cdot \boldsymbol{S}_j\rangle\langle\tau_i^l\tau_j^l\rangle]$. The results are presented in Fig. 2(c). Spin and orbital sectors are decoupled at $j_D = 0$, and are strongly entangled near and above j_{Dc}. This is consistent with the picture where the spin singlet and the parallel PS configuration are realized as a quantum mechanical superposition.

To examine a connection of the newly finding spin-orbital resonant state with the well-known spin ordered state in the honeycomb-lattice Heisenberg model, we introduce the artificial field acting on the orbital-lattice sector. This Hamiltonian is given by $\mathcal{H}_M = -h_M \sum_i \sigma_i^z \otimes F_i$ where $(F)_{\nu\nu'} = \frac{i}{\sqrt{3}}\sum_l \varepsilon_{l\nu\nu'}$ is a 3×3 matrix. This field lifts the doublet ground state for $\mathcal{H}_{\mathrm{JT}}$, and reduces the low-energy effective model into the AFM Heisenberg model without the orbital degree of freedom. The phase diagram on a plane of j_D and h_M

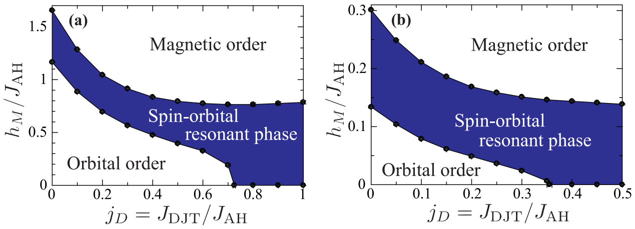

FIG. 3: (color online). (a) Phase diagram on the plane of $J_{\rm DJT}/J_{\rm AH}$ and $h_{\mathcal{M}}/J_{\rm AH}$. The interaction between the octahedra, $\mathcal{H}_{\rm inter}$, is taken into account in (b), where the parameter is chosen to be $K/J_{\rm AH} = 0.1$.

is shown in Fig. 3(a). The Néel order appears for large h_M. We find the spin-orbital resonant state is realized in between the spin ordered state and the orbital ordered state which is realized in small j_D and h_M.

The spin-orbital resonant state is realized in more realistic parameter space, when the lattice effect is taken into account beyond the independent octahedra approximation. The interactions between the $\rm O_6$ octahedra are modeled by the Hamiltonian: $\mathcal{H}_{\rm inter} = K/(4\rho_0^2)\sum_{\langle ij\rangle_l}(3Q^l_{iu}Q^l_{ju} - Q^l_{iv}Q^l_{jv})$ where $Q^l_{iu} = \cos(2n_l\pi/3)Q_{iu} + \sin(2n_l\pi/3)Q_{iv}$ and $Q^l_{iv} = -\sin(2n_l\pi/3)Q_{iu} + \cos(2n_l\pi/3)Q_{iv}$. This is derived from the elastic interaction between the two O ions belonging to the NN octahedra, and K is the spring constant. The numerical results for $\mathcal{H}_{\rm eff} + \mathcal{H}_{\rm inter}$ are presented in Fig. 3(b). The spin-orbital resonant phase is shifted to the lower side of j_D and h_M. In particular, without the artificial field ($h_M = 0$), j_{Dc} is decreased down to 0.35. This result satisfies the condition of $j_D < 0.5$, in which $\mathcal{H}_{\rm JT}$ is valid as an effective Hamiltonian for the low-energy vibronic states of $\mathcal{H}_{\rm rot}$.

From the above analyses, it turns out that the present finding spin-orbital resonant state emerges under the quantum orbital state, and a stability of this state is controlled by the DJT effect. We have found previously in Ref. [20] that, in the honeycomb lattice orbital-only model, $\mathcal{H}_{\rm orb} = J\sum_{\langle ij\rangle_l}\tau^l_i\tau^l_j$, conventional long-range orders, as well as any translational-symmetry broken states, are found neither in quantum calculations at zero temperature nor in finite-temperature classical calculations. A suggested ground state is a resonant orbital state, i.e., a superposition of the states where a honeycomb lattice is covered by the NN bond dimers with the parallel PS configuration. Here, we connect the present exchange Hamiltonian $\mathcal{H}_{\rm exch}$ in Eq. (1) to $\mathcal{H}_{\rm orb}$, and examine the relation between the two resonant states. For this end, we generalize the electron transfer as $t_{pd} \to t_{pd}(\eta)$ by introducing a parameter η, and apply the staggered magnetic field as $\mathcal{H}_h = -h\sum_i(-1)^i S^z_i$. Detailed models are given in SM [14]. The present SE Hamiltonian $\mathcal{H}_{\rm exch}$ and the orbital-only model $\mathcal{H}_{\rm orb}$ correspond to $(\eta, h) = (\pi/3, 0)$ and $(\pi/2, \infty)$, respectively, and the orbital states between the two limits are examined continuously. In Fig. 4, a three-dimensional plot for the phase diagram as functions of h, η and j_D is presented. The spin-orbital resonant state at $(\eta, h) = (\pi/3, 0)$ and $j_D > j_{Dc} = 0.75$ continuously connects to the orbital resonant state in the orbital-only model realized in $(\eta, h) = (\pi/2, \gg J_{AH})$. This fact implies that the present spin-orbital state belongs to the same class of the orbital resonance state in the orbital-only model, and supports the picture shown in Fig. 1(c). We note that a stability of the orbital resonant state in $\mathcal{H}_{\rm orb}$ was examined by using several calculation methods and was confirmed at the infinite size limit [20]. We strongly suppose that the spin-orbital resonant state also does not break translational-symmetries, and is survived beyond the present finite-size calculations.

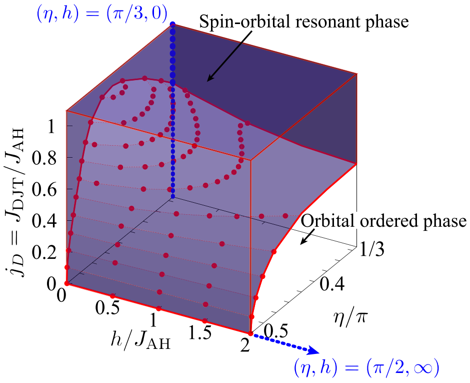

FIG. 4: (color online). Phase diagram for the model where the generalization of the electron transfer, η, and the staggered magnetic field, h, are taken into account [see text]. The SE interaction model $\mathcal{H}_{\rm exch}$ and the orbital-only model $\mathcal{H}_{\rm orb}$ correspond to $(\eta, h) = (\pi/3, 0)$ and $(\pi/2, \infty)$, respectively. A shaded area shows the spin-orbital resonant phase.

Based on the theoretical calculations, we propose a possible scenario for $\rm Ba_3CuSb_2O_9$ [7, 8]. The x-ray experimental results suggest a kind of short-range honeycomb-lattice domain of the order of 10Å, which justifies the present finite-size cluster analyses to mimic the realistic situation. The observed positive Weiss constant is not trivial in orbital degenerate magnets where the ferromagnetic interaction is usually dominant, and can be explained by the present calculation where the exchange paths are properly taken into account in a realistic lattice structure. For the no long-range spin and orbital orders in the hexagonal samples, the present spin-orbital resonant state is one plausible candidate. The temperature dependence of the magnetic susceptibility is decomposed into the Curie tail and a gapped component. When the former is attributed to the orphan spins, the latter is consistent with the present spin-orbital resonant state where the short-range spin singlets are realized. This interpretation is also applicable to the electronic specific heat; the peak around 20K, which is robust against the magnetic field, is associated with the spin-orbital resonant state, and the low temperature component is due to the orphan spins. The existence of the gapped magnetic excitation is also suggested by the nuclear magnetic resonance measurements [21]. A detailed magnetic structure is revealed by the inelastic neutron scattering; a finite excitation-energy spectrum, interpreted as a singlet-triplet excitation, shows a characteristic momentum dependence which does not indicate a simple local NN singlet pairs, but some spatial distribution. This might be explained in the present spin-orbital resonant state, where the spin-singlet pairs are not localized, but are shuffled quantum mechanically together with the orbital configuration. The time scale for the spin-orbital motion in the spin-orbital resonant is governed by the local DJT effect $\omega^2/E_{\rm JT}$ ~1-10meV and the inter-site exchange interaction J ~1-10meV, both of which are in between the ESR time scale ($\sim 10^{-9}$s) and the x-ray time scale ($\sim 10^{-15}$s). These relations are suitable for the experiments which seems to be contradicted with each other at a glance: the almost isotropic ESR signal and the anisotropic extended x-ray absorption fine structure (EXAFS) data. Further comparison between the theory and experiments are necessary to confirm the spin-orbital resonant picture. The vibronic excitations measured by Raman and x-ray scattering spectroscopies are possible methods to check the scenario.

In summary, we find that the spin-orbital resonant state is realized by the DJT effect in a honeycomb lattice spin-orbital model. Rearrangements of the spin-singlet pairs and the parallel orbital PS configurations are strongly entangled with each other. From the viewpoint of the orbital ordered state, the DJT effect strengthens the orbital fluctuation, diminishes the local orbital moment, and then induces the spin orbital resonant state. The present study does not only provides systematic explanations for the recent experiments in $\mathrm{Ba_3CuSb_2O_9}$, but also proposes a new route to the spin-liquid state in spin-orbital coupled systems where the dynamical JT effect is relevant.

We thank S. Nakatsuji, H. Sawa, M. Hagiwara and Y. Wakabayashi for helpful discussions. This work was supported by KAKENHI from MEXT and Tohoku University "Evolution" program. JN is supported by the global COE program "Weaving Science Web beyond Particle-Matter Hierarchy" of MEXT, Japan. Parts of the numerical calculations are performed in the supercomputing systems in ISSP, the University of Tokyo.

---

[1] L. Balents, Nature **464**, 199 (2010).
[2] Y. Shimizu, *et al.*, Phys. Rev. Lett. **91**, 107001 (2003).
[3] J. S. Helton, *et al.*, Phys. Rev. Lett. **98**, 107204 (2007).
[4] N. Read and S. Sachdev, Phys. Rev. Lett. **66**, 1773 (1991).
[5] H. Tsunetsugu, *et al.*, J. Phys. Soc. Jpn. **75**, 083701 (2006).
[6] T. Senthil, *et al.*, Phys. Rev. B **62**, 7850 (2000).
[7] H. Zhou, *et al.*, Phys. Rev. Lett. **106**, 147204 (2011).
[8] S. Nakatsuji, *et al.*, Science **336**, 559 (2012).
[9] L. F. Feiner, *et al.*, Phys. Rev. Lett. **78**, 2799 (1997).
[10] G. Khaliullin and V. Oudovenko, Phys. Rev. Lett. **56**, R14243 (1997).
[11] Y. Q. Li, *et al.*, Phys. Rev. Lett. **81**, 3527 (1998).
[12] L. Thompson and P. A. Lee, arXiv:1202.5655.
[13] P. Corboz, *et al.*, arXiv:1207.6029.
[14] Supplemental Material http://link.aps.org/supplemental/.
[15] M. C. M. O'Brien, Proc. Roy. Soc. (London) **A281**, 323 (1964).
[16] The axes of coordinate, x, y, z, are chosen to be parallel to the orthogonal Cu-O bond directions in an octahedron. Since the exchange paths are identified by a plane (lm), a NN Cu-Cu bond is labeled by an index n, where (l, m, n) are the cyclic permutations of the Cartesian coordinates.
[17] Y. Mizuno, *et al.*, Phys. Rev. B **57**, 5326 (1998).
[18] K. Kugel and D. Khomskii, Usp. Fiz. Nauk **136**, 621 (1982) [Sov. Phys. Usp. **25**, 231 (1982)].
[19] J. S. Koehler and D. M. Dennison, Phys. Rev. **57**, 1006 (1940)
[20] J. Nasu, *et al.*, Phys. Rev. B **78**, 024416 (2008).
[21] J. A. Quilliam, *et al.*, arXiv:1207.6469.

Supplemental Material: Dynamical Jahn-Teller Effect in Spin-Orbital Coupled System

In this Supplemental Material, detailed derivations of the superexchange Hamiltonian and the effective vibronic Hamiltonian are presented.

SUPEREXCHANGE HAMILTONIAN

In this section, a derivation and explicit forms of the superexchange Hamiltonian in Eq. (1) in the main article are presented.

Derivation of the superexchange Hamiltonian

We consider a two-dimensional honeycomb lattice where a CuO$_6$ octahedron is located in each site as shown in Fig. 1(a) in the main article. An octahedron and a Cu site are labeled by an index i and their positions are denoted by $\boldsymbol{r}_i$. The O sites which belong to the i-th octahedra are labeled by the indexes i and $\delta(=\pm x, \pm y, \pm z)$. Positions of these O sites are $\boldsymbol{r}_i + \boldsymbol{d}_\delta$, where $\boldsymbol{d}_\delta$ is a vector along a direction δ with an amplitude of the nearest neighbor (NN) Cu-O bond distance. The axes of coordinates, x, y, z, are taken to be along the NN Cu-O bond directions in an octahedron as shown in Fig. 1(a) in the main article. A NN Cu-Cu bond, where the exchange paths are located on the lm-plane (see Fig. 5), is labeled by an index n, where (l, m, n) are the cyclic permutations of the Cartesian coordinates.

We start from the dp-type Hamiltonian where the doubly-degenerate e_g orbitals in Cu sites and the three $2p$ orbitals in O sites are introduced. The Hamiltonian is given by

$$\mathcal{H}_{pd} = \mathcal{H}_t + \mathcal{H}_\Delta + \mathcal{H}_{Ud} + \mathcal{H}_{Up}. \tag{3}$$

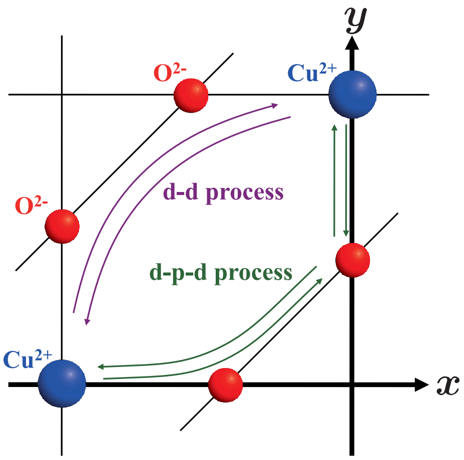

FIG. 5: Schematic two-types of the exchange processes on the xy plane.

The first term represents the electron transfer between the Cu and O orbitals and that between the O orbitals:

$$\mathcal{H}_t = -\sum_{i\delta}\sum_{\gamma\eta\sigma}\left(t^{\gamma\eta}_{dp;i\delta} d^\dagger_{i\gamma\sigma} p_{i\delta\eta\sigma} + H.c.\right) - \sum_{<i\delta;j\delta'>}\sum_{\eta\eta'\sigma}\left(t^{\eta\eta'}_{pp;i\delta j\delta'} p^\dagger_{i\delta\eta\sigma} p_{j\delta'\eta'\sigma} + H.c.\right), \tag{4}$$

where $d_{i\gamma\sigma}$ is the annihilation operator for a Cu hole at the i-th octahedron with orbital $\gamma(=3z^2-r^2, x^2-y^2)$ and spin $\sigma(=\uparrow, \downarrow)$, and $p_{i\delta\eta\sigma}$ is the annihilation operator for an O hole at the δ-th O site in the i-th octahedron with orbital $\eta(=x, y, z)$ and spin σ. A symbol $< i\delta; j\delta' >$ represents the NN O sites labeled by (i, δ) and (j, δ'), and $t^{\gamma\eta}_{dp;i\delta}$ and $t^{\eta\eta'}_{pp;i\delta j\delta'}$ are the corresponding transfer integrals. The second term in Eq. (3) represents the energy differences given by

$$\mathcal{H}_\Delta = \sum_{i\delta}\left[(\Delta+\Delta_p)\, n^p_{i\delta\eta_\delta} + (\Delta-\Delta_p)\sum_{\eta\neq\eta_\delta} n^p_{i\delta\eta}\right], \tag{5}$$

where $n^p_{i\delta\eta}(\equiv \sum_\sigma p^\dagger_{i\delta\eta\sigma} p_{i\delta\eta\sigma})$ is the number operator, and η_δ indicates the $2p_{|\delta|}$ orbital. The first (second) term represents the energy difference between the Cu e_g and O $2p$ orbitals, which (do not) form the σ bond, and Δ and Δ_p are the energy parameters. The third and fourth terms in Eq. (3) represent the on-site electron-electron interactions in the Cu and O sites, respectively. These are given by

$$\begin{aligned}\mathcal{H}_{Ud} &= U_d \sum_{i\gamma} d^\dagger_{i\gamma\uparrow} d_{i\gamma\uparrow} d^\dagger_{i\gamma\downarrow} d_{i\gamma\downarrow} \\ &+ U'_d \sum_{i\sigma\sigma'}\sum_{\gamma>\gamma'} d^\dagger_{i\gamma\sigma} d_{i\gamma\sigma} d^\dagger_{i\gamma'\sigma'} d_{i\gamma'\sigma'} \\ &- J_d \sum_{i\sigma\sigma'}\sum_{\gamma>\gamma'} d^\dagger_{i\gamma\sigma} d_{i\gamma\sigma'} d^\dagger_{i\gamma'\sigma'} d_{i\gamma'\sigma} \\ &- J'_d \sum_{i}\sum_{\gamma>\gamma'}\left(d^\dagger_{i\gamma\uparrow} d_{i\gamma\downarrow} d^\dagger_{i\gamma'\uparrow} d_{i\gamma'\downarrow} + \text{H.c.}\right),\end{aligned} \tag{6}$$

and

$$\begin{aligned}\mathcal{H}_{Up} &= U_p \sum_{i\delta\eta} p^\dagger_{i\delta\eta\uparrow} p_{i\delta\eta\uparrow} p^\dagger_{i\delta\eta\downarrow} p_{i\delta\eta\downarrow} \\ &+ U'_p \sum_{i\delta\sigma\sigma'}\sum_{\eta>\eta'} p^\dagger_{i\delta\eta\sigma} p_{i\delta\eta\sigma} p^\dagger_{i\delta\eta'\sigma'} p_{i\delta\eta'\sigma'} \\ &- J_p \sum_{i\delta\sigma\sigma'}\sum_{\eta>\eta'} p^\dagger_{i\delta\eta\sigma} p_{i\delta\eta\sigma'} p^\dagger_{i\delta\eta'\sigma'} p_{i\delta\eta'\sigma} \\ &- J'_p \sum_{i\delta}\sum_{\eta>\eta'}\left(p^\dagger_{i\delta\eta\uparrow} p_{i\delta\eta\downarrow} p^\dagger_{i\delta\eta'\uparrow} p_{i\delta\eta'\downarrow} + \text{H.c.}\right),\end{aligned} \tag{7}$$

where U_d (U_p), U'_d (U'_p), J_d (J_p) and J'_d (J'_p) are the intra-orbital Coulomb interaction, the inter-orbital Coulomb interaction, the Hund coupling and the pair-hopping interaction for the d (p) electrons, respectively. We assume the conditions $U_d = U'_d - 2J_d$ and $J'_d = J_d$ in Eq. (6).

From the dp-type Hamiltonian, the superexchange interactions between the NN Cu sites are obtained by the perturbational expansion. The exchange processes are classified into the two processes; two holes occupy virtually the same Cu (O) site in the intermediate states, termed the dd (dpd) processes as shown in Fig. 5. The superexchange interactions for the NN ij sites labeled by l through the dd processes are given by

$$\begin{aligned}\mathcal{H}_{dd}^{ij(l)} =& - A_d \left(\frac{5}{4} - 5\tau_i^l\tau_j^l + 3\bar{\tau}_i^l\bar{\tau}_j^l + 3T_i^yT_j^y \right) P_{ij}^T \\ &-B_d \left(\frac{5}{2} - 2\tau_i^l - 2\tau_j^l - 6T_i^yT_j^y \right) P_{ij}^S \\ &-C_d \left(\frac{5}{4} - 2\tau_i^l - 2\tau_j^l + 5\tau_i^l\tau_j^l - 3\bar{\tau}_i^l\bar{\tau}_j^l + 3T_i^yT_j^y \right) P_{ij}^S,\end{aligned} \tag{8}$$

where $A_d = t_p'^2 t_d^4/[\Delta^4(U_d' - J_d)]$, $B_d = t_p'^2 t_d^4/[\Delta^4(U_d' + J_d)]$, and $C_d = t_p'^2 t_d^4/[\Delta^4(U_d + J_d)]$. The transfer integrals t_d and t_p' are defined by the Slater-Koster parameters as $-t_d = (pd\sigma)$ and $-t_p' = \frac{1}{2}(pp\sigma) - \frac{1}{2}(pp\pi)$, respectively. [1] The spin-singlet and spin-triplet operators are introduced by $P_{ij}^T = \frac{3}{4} + \boldsymbol{S}_i \cdot \boldsymbol{S}_j$ and $P_{ij}^S = \frac{1}{4} - \boldsymbol{S}_i \cdot \boldsymbol{S}_j$, respectively, where $\boldsymbol{S}_i$ is the spin operator with an amplitude of 1/2 at site i. The orbital degree of freedom in a Cu ion is represented by the pseudo-spin operator $\boldsymbol{T}_i$ with an amplitude of $1/2$. For convenience, we introduce $\tau_i^l = \cos(2\pi n_l/3)T_i^z - \sin(2\pi n_l/3)T_i^x$ and $\bar{\tau}_i^l = \cos(2\pi n_l/3)T_i^x + \sin(2\pi n_l/3)T_i^z$ with $(n_z, n_x, n_y) = (0, 1, 2)$. The eigen state of τ^l with the eigen value of +1/2 (-1/2) corresponds to the state where $d_{3l^2-r^2}$ ($d_{m^2-n^2}$) orbital is occupied by a hole. In the same way, the exchange interactions through the dpd processes are given by

$$\begin{aligned}\mathcal{H}_{dpd}^{ij(l)} =& - A_p \left(4 - 4\tau_i^l - 4\tau_j^l + 4\tau_i^l\tau_j^l - 12\bar{\tau}_i^l\bar{\tau}_j^l\right) P_{ij}^T \\ &- (B_p + 2C_p) \\ &\times \left(4 - 4\tau_i^l - 4\tau_j^l + 4\tau_i^l\tau_j^l - 12\bar{\tau}_i^l\bar{\tau}_j^l\right) P_{ij}^S,\end{aligned} \tag{9}$$

where $A_p = t_p'^2 t_d^4/[\Delta^4(U_p' - J_p + 2\Delta)]$, $B_p = t_p'^2 t_d^4/[\Delta^4(U_p' + J_p + 2\Delta)]$ and $C_p = t_p^2 t_d^4 (U_p + 2\Delta - \Delta_p)/[\Delta^4\{(U_p + 2\Delta)^2 - J_p'^2 - \Delta_p^2\}]$. The transfer integral t_p is defined by the Slater-Koster parameters as $-t_p = \frac{1}{2}(pp\sigma) + \frac{1}{2}(pp\pi)$. [1]

The two-types of the superexchange Hamiltonians are now taken together:

$$\begin{aligned}\mathcal{H}_{\rm exch} =& \sum_{<ij>_l} \left(\mathcal{H}_{dd}^{ij(l)} + \mathcal{H}_{dpd}^{ij(l)} \right) \\ =& \sum_{<ij>_l} \Big[J_{ss}\boldsymbol{S}_i \cdot \boldsymbol{S}_j + J_{\tau\tau}\tau_i^l\tau_j^l + J_{\bar{\tau}\bar{\tau}}\bar{\tau}_i^l\bar{\tau}_j^l + J_{yy}T_i^yT_j^y \\ &+ J_{ss\tau}\boldsymbol{S}_i \cdot \boldsymbol{S}_j(\tau_i^l + \tau_j^l) + J_{ss\tau\tau}\boldsymbol{S}_i \cdot \boldsymbol{S}_j\tau_i^l\tau_j^l \\ &+ J_{ss\bar{\tau}\bar{\tau}}\boldsymbol{S}_i \cdot \boldsymbol{S}_j\bar{\tau}_i^l\bar{\tau}_j^l + J_{ssyy}\boldsymbol{S}_i \cdot \boldsymbol{S}_jT_i^yT_j^y \Big],\end{aligned} \tag{10}$$

where the exchange parameters are defined by $J_{ss} = -\frac{5}{4}A_d - 4A_p + \frac{5}{2}B_d + 4B_p + \frac{5}{4}C_d + 8C_p$, $J_{\tau\tau} = \frac{15}{4}A_d - 3A_p - B_p - \frac{5}{4}C_d - 2C_p$, $J_{\bar{\tau}\bar{\tau}} = -\frac{9}{4}A_d + 9A_p + 3B_p + \frac{3}{4}C_d + 6C_p$, $J_{yy} = -\frac{9}{4}A_d + \frac{3}{2}B_d - \frac{3}{4}C_d$, $J_{ss\tau} = 4A_p - 2B_d - 4B_p - 2C_d - 8C_p$, $J_{ss\tau\tau} = 5A_d - 4A_p + 4B_p + 5C_d + 8C_p$, $J_{ss\bar{\tau}\bar{\tau}} = -3A_d + 12A_p - 12B_p - 3C_d - 24C_p$ and $J_{ssyy} = -3A_d - 6B_d + 3C_d$.

We estimate the exchange constants quantitatively. By using the realistic parameter values, [2] $t_d = 1.2$eV, $t_p = t_p' = -0.65$eV, $U_d' = 6$eV, $U_p = 4$eV, $U_p' = 3$eV, $J_d/U_d' = J_p/U_p' = 0.5$, $\Delta = 3$eV and $\Delta_p = 0.1$eV, we have $J_{\tau\tau}/J_{ss} = 0.78$, $J_{ss\tau\tau}/J_{ss} = 4.5$, $J_{ss\tau}/J_{ss} = 1.7$, $J_{\bar{\tau}\bar{\tau}}/J_{ss} = 2.3$, $J_{ss\bar{\tau}\bar{\tau}}/J_{ss} = -5.2$, $J_{yy}/J_{ss} = -0.89$, and $J_{ssyy}/J_{ss} = -3.1$ as a unit of $J_{ss} = 6.5$meV. These values are adopted to analyze the spin and orbital states in the two NN Cu sites. In the numerical calculations for $\mathcal{H}_{\rm eff} = \mathcal{H}_{\rm exch} + \mathcal{H}_{\rm JT}$ in the main article, we adopt the above ratios of the exchange constants as a unit of $J_{ss}/J_{\rm AH} = 0.15$.

Generalization of the superexchange interaction

In the main article, we examine the connection between the superexchange Hamiltonian in Eq. (10) and the honeycomb-lattice orbital-only model given by

$$\mathcal{H}_{\rm orb} = J \sum_{\langle ij \rangle_l} \tau_i^l \tau_j^l, \tag{11}$$

by generalizing the electron transfer integrals as follows. We modify the transfer integral between the p_x and $d_{3z^2-r^2}$ orbitals and that between p_x and $d_{x^2-y^2}$ along the x direction as $(t_{pd;ix}^{3z^2-r^2,x}, t_{pd;ix}^{x^2-y^2,x}) = (-t_d/2, t_d\sqrt{3}/2) \rightarrow (t_{pd;ix}^{3z^2-r^2,x}(\eta), t_{pd;ix}^{x^2-y^2,x}(\eta)) = (-t_d\cos\eta, t_d\sin\eta)$ by introducing a parameter η. The transfer integrals between other orbitals and those along other directions are obtained by the symmetry considerations. The generalized transfer integrals at $\eta = \pi/3$ reproduce the original transfer integrals. At $\eta = \pi/2$, we have $[t_{pd;ix}^{3z^2-r^2,x}(\eta = \pi/2), t_{pd;ix}^{x^2-y^2,x}(\eta = \pi/2)] = (0, t_d)$, i.e. the electron transfer between the p_x and $d_{3z^2-r^2}$ orbitals along z vanishes.

Through the generalization of the transfer integrals, we derive the superexchange Hamiltonian. The generalized exchange constants are given by $J_{ss}(\eta) = -A_d - 4A_p + 2B_d + 4B_p + C_d + 8C_p + (-A_d + 2B_d + C_d)\cos^2 2\eta$, $J_{\tau\tau}(\eta) = 3A_d - C_d + (3A_d - 12A_p - 4B_p - C_d - 8C_p)\cos^2 2\eta$, $J_{\bar{\tau}\bar{\tau}}(\eta) = (-3A_d + 12A_p + 4B_p + C_d + 8C_p)\sin^2 2\eta$, $J_{yy}(\eta) = -(3A_d - 2B_d + C_d)\sin^2 2\eta$, $J_{ss\tau}(\eta) = 4(2A_p - B_d - 2B_p - C_d - 4C_p)\cos 2\eta$, $J_{ss\tau\tau}(\eta) = 4(A_d + C_d + (A_d - 4A_p + 4B_p + C_d + 8C_p)\cos^2 2\eta)$, $J_{ss\bar{\tau}\bar{\tau}}(\eta) = -4(A_d - 4A_p + 4B_p + C_d + 8C_p)\sin^2 2\eta$, and $J_{ssyy}(\eta) = -4(A_d + 2B_d - C_d)\sin^2 2\eta$. At $\eta = \pi/2$, the superexchange Hamiltonian is given by

$$\begin{aligned}\mathcal{H}_{\rm exch} =& \sum_{<ij>_l} \big[J_{ss}\boldsymbol{S}_i \cdot \boldsymbol{S}_j + J_{\tau\tau}\tau_i^l\tau_j^l \\ &+ J_{ss\tau}\boldsymbol{S}_i \cdot \boldsymbol{S}_j(\tau_i^l + \tau_j^l) + J_{ss\tau\tau}\boldsymbol{S}_i \cdot \boldsymbol{S}_j\tau_i^l\tau_j^l \big].\end{aligned} \tag{12}$$

To reproduce the orbital-only model, we further introduce the staggered magnetic field defined by

$$\mathcal{H}_h = -h\sum_i (-1)^i S_i^z. \tag{13}$$

In the limit of $h \to \infty$, the spin degree of freedom is frozen, and Eq. (12) is reduced to the orbital-only model in Eq. (11). The exchange constant J corresponds to $J_{\tau\tau}(\eta = \pi/2) - J_{ss\tau\tau}(\eta = \pi/2)/4$ which is negative.

VIBRONIC HAMILTONIAN

In this section, a detailed derivation of the effective vibronic Hamiltonian in Eq. (2) in the main article is presented.

Derivation of the effective vibronic Hamiltonian

We start from the electron-lattice interaction Hamiltonian introduced in the main article. The two vibrational modes, Q_u and Q_v, with the E symmetry couple with the e_g electronic orbitals. This is given by

$$\mathcal{H}_{e\text{-}l} = \sum_i \Bigg[-\frac{1}{2M}\left(\frac{\partial^2}{\partial Q_{ui}^2} + \frac{\partial^2}{\partial Q_{vi}^2}\right) + \frac{M\omega^2}{2}\rho_i^2 \\ + 2A(T_i^x Q_{vi} + T_i^z Q_{ui}) + B(Q_{ui}^3 - 3Q_{vi}^2 Q_{ui}) \Bigg], \tag{14}$$

where $\rho_i = \sqrt{Q_{ui}^2 + Q_{vi}^2}$ is an amplitude of the lattice distortion at the i-th octahedron. The first two terms are for the harmonic vibrations with frequency ω and oxygen mass M. The third term describes the Jahn-Teller (JT) coupling with a coupling constant $A(>0)$, and the last term represents the anharmonic lattice potential, where B is negative.

We analyze this Hamiltonian based on the Born-Oppenheimer approximation. The vibronic wave-function is written as a product of the electronic wave function, ψ_k, and the lattice wave function, ϕ_λ^k, as $\Phi_{\lambda,k}(\boldsymbol{r},\boldsymbol{Q}) = \psi_k(\boldsymbol{r},\boldsymbol{Q})\phi_\lambda^k(\boldsymbol{Q})$, where $\boldsymbol{r}$ and $\boldsymbol{Q}$ are the electron and lattice coordinates, respectively, and k and λ describe the electronic and vibrational states, respectively. The adiabatic potentials for an octahedron are given as

$$U^{(k=\pm)} = \frac{M\omega^2\rho^2}{2} \pm A\rho + B\rho^3\cos\theta, \tag{15}$$

where $\theta \equiv \tan^{-1}(Q_v/Q_u)$. The wave functions for a hole corresponding to the lower adiabatic potential, i.e. $k = -$, is given as

$$\psi_-(\boldsymbol{r},\theta) = \psi_{x^2-y^2}(\boldsymbol{r})\cos\frac{\theta}{2} - \psi_{3z^2-r^2}(\boldsymbol{r})\sin\frac{\theta}{2}. \tag{16}$$

In the case of $B = 0$, $U^{(-)}$ takes its minimum of $E_{\rm JT} = A^2/(2M\omega^2)$ at $\rho = \rho_0 \equiv A/(M\omega^2)$ for any θ. When B is taken into account, the potential takes its minima (maxima) at angles $\theta_{\mu\nu} = \mu\pi + 2\nu\pi/3$ with integers $\mu = 0$ ($\mu = 1$) and $\nu = (0, 1, 2)$, as shown in Fig. 1(b) in the main article.

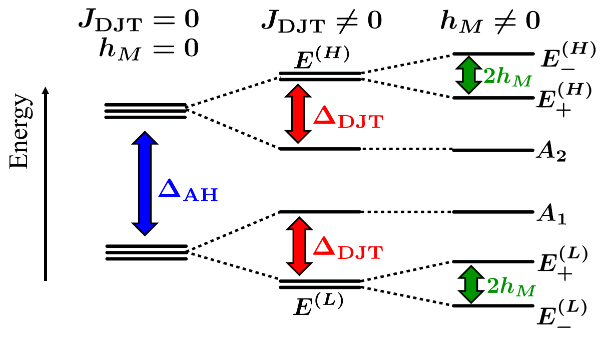

FIG. 6: The energy level scheme for the vibronic states.

Here we assume that the zero-point vibration energy ($\omega/2$) is sufficiently smaller than the JT energy ($E_{\rm JT}$), and the vibronic motion is confined on the lower adiabatic potential. Then, the effective Hamiltonian is given by

$$\begin{aligned}\mathcal{H}_{\rm vib} &= \int d\boldsymbol{r}\psi_-(\boldsymbol{r},\boldsymbol{Q})^* \left[-\frac{1}{2M}\left(\frac{\partial^2}{\partial Q_u^2} + \frac{\partial^2}{\partial Q_v^2}\right) + U^{(-)}\right] \\ &\quad \times \psi_-(\boldsymbol{r},\boldsymbol{Q}) \\ &= \frac{1}{\sqrt{\rho}}\left[-\frac{1}{2M}\frac{\partial^2}{\partial\rho^2} + \frac{M\omega^2}{2}(\rho-\rho_0)^2 - E_{\rm JT}\right]\sqrt{\rho} \\ &\quad - \frac{1}{2M\rho^2}\frac{\partial^2}{\partial\theta^2} + B\rho^3\cos 3\theta. \end{aligned} \tag{17}$$

The vibronic motion is classified into the radial mode where the amplitude ρ varies around ρ_0, and the rotational mode where the angle θ varies at $\rho = \rho_0$. We consider the case that the excitation energy for the radial mode, ω, is larger than the kinetic energy for rotational mode, $1/(2M\rho_0^2) = \omega^2/(4E_{\rm JT})$, and focus on the rotational mode, corresponding to the last two terms in Eq. (17). The effective Hamiltonian for the rotational mode is defined as

$$\mathcal{H}_{\rm rot} = -\frac{1}{2M\rho_0^2}\frac{\partial^2}{\partial\theta^2} + B\rho_0^3\cos 3\theta. \tag{18}$$

Since this Hamiltonian describes the kinetic motion under the periodic potential, solutions of the Schrödinger equation, $\mathcal{H}_{\rm rot}\phi_\lambda(\theta) = \varepsilon_\lambda\phi_\lambda(\theta)$, are obtained as the Bloch states. [3, 4] As shown in Fig. 6, the lowest-six eigen states are labeled by the irreducible representation in the C_{3v} group, $E^{(L)}$, A_1, A_2 and $E^{(H)}$, where $E^{(L)}$ and $E^{(H)}$ are the doubly degenerate representations and the degenerate bases are labeled by the indexes $+$ and $-$. From the Bloch-type eigen states, we introduce the Wannier-type wave functions. From the lowest-six eigen states, we introduce the six Wannier functions, $\phi_{0\nu}(\theta)$ and $\phi_{1\nu}(\theta)$ ($\nu = 0, 1, 2$), which are almost localized around $\theta_{0\nu}$ and $\theta_{1\nu}$ respectively. Explicit relations between the Bloch functions and the Wannier functions are given by $\phi_{E_\pm^{(L)}} = (\phi_{00} + e^{\pm 2i\pi/3}\phi_{01} + e^{\pm 4i\pi/3}\phi_{02})/\sqrt{3}$,

$\phi_{A_1} = (\phi_{00}+\phi_{01}+\phi_{02})/\sqrt{3}$, $\phi_{A_2} = (\phi_{10}+\phi_{11}+\phi_{12})/\sqrt{3}$ and $\phi_{E_{\pm}^{(H)}} = (\phi_{10}+e^{\pm 2i\pi/3}\phi_{11}+e^{\pm 4i\pi/3}\phi_{12})/\sqrt{3}$. Because of the parity of the wave functions, the two spaces based on the wave functions $\phi_{0\nu}(\theta)$ and $\phi_{1\nu}(\theta)$, termed the μ=0 and 1 spaces, respectively, are orthogonal with each other and are treated independently.

The vibronic wave-function is represented by a product form of $\Phi_{\mu\nu}(\boldsymbol{r};\theta) = \psi_{-}(\boldsymbol{r};\theta)\phi_{\mu\nu}(\theta)$. For simplicity, we assume that the energy difference between the $E^{(L)}$ and A_1 states is equal to that between A_2 and $E^{(H)}$. We denote this energy difference by Δ_{DJT} and that between the A_1 and A_2 states by Δ_{AH}. Then, the low-energy vibronic Hamiltonian is obtained as a simple form:

$$\begin{aligned}\mathcal{H}_{\mathrm{JT}} = & \left(\Delta_{\mathrm{DJT}} + \frac{\Delta_{\mathrm{AH}}}{2}\right) \\ & \times \Big(-|\Phi_{E_{+}^{(L)}}\rangle\langle\Phi_{E_{+}^{(L)}}| - |\Phi_{E_{-}^{(L)}}\rangle\langle\Phi_{E_{-}^{(L)}}| \\ & \quad |\Phi_{E_{+}^{(H)}}\rangle\langle\Phi_{E_{+}^{(H)}}| + |\Phi_{E_{-}^{(H)}}\rangle\langle\Phi_{E_{-}^{(H)}}|\Big) \\ & + \frac{\Delta_{\mathrm{AH}}}{2}\left(-|\Phi_{A_1}\rangle\langle\Phi_{A_1}| + |\Phi_{A_2}\rangle\langle\Phi_{A_2}|\right). \end{aligned} \tag{19}$$

This is rewritten in the Wannier function representation as

$$\mathcal{H}_{\mathrm{JT}} = \frac{1}{2}\sum_{i}\sum_{l=0}^{2}\sigma_i^z \otimes \left(J_{\mathrm{DJT}}D_i^l - \frac{J_{\mathrm{AH}}}{2}D_i^{l2}\right), \tag{20}$$

where the 2×2 matrix σ_i^z is the z component of the Pauli matrices, and is defined for the index μ. We define $J_{\mathrm{DJT}} = 2\Delta_{\mathrm{DJT}}/3$ and $J_{\mathrm{AH}} = 4\Delta_{\mathrm{DJT}}/3 + \Delta_{\mathrm{AH}}$, by which the condition $J_{\mathrm{DJT}}/J_{\mathrm{AH}} < 1/2$ is derived.

We introduce the 3×3 matrices $(D^l)_{\nu\nu'} = |\varepsilon_{l\nu\nu'}|$, where $\varepsilon_{l\nu\nu'}$ are the Levi-Civita completely antisymmetric tensors, for the index ν. By using the matrices, we have

$$\sum_{l=0}^{2} D_i^l = \begin{array}{c} \begin{array}{ccc} \Phi_{\mu 0} & \Phi_{\mu 1} & \Phi_{\mu 2} \end{array} \\ \begin{pmatrix} 0 & 1 & 1 \\ 1 & 0 & 1 \\ 1 & 1 & 0 \end{pmatrix} \end{array}, \tag{21}$$

$$\sum_{l=0}^{2} D_i^{l2} = 2\begin{array}{c} \begin{array}{ccc} \Phi_{\mu 0} & \Phi_{\mu 1} & \Phi_{\mu 2} \end{array} \\ \begin{pmatrix} 1 & 0 & 0 \\ 0 & 1 & 0 \\ 0 & 0 & 1 \end{pmatrix} \end{array}. \tag{22}$$

On an equal footing of the effective vibronic Hamiltonian in Eq. (20), we provide a representation for the superexchange Hamiltonian, where the six vibronic wave functions, $\Phi_{\mu\nu}$ $(\mu = 0,1; \nu = 0,1,2)$, are adopted as a basis set. This is performed by introducing the projection operator as $\mathcal{H}_{\mathrm{exch}} \to \mathcal{P}\mathcal{H}_{\mathrm{exch}}\mathcal{P}$. Here $\mathcal{P}$ operates the vibronic wave function so as to be restricted within the six basis functions $\Phi_{\mu\nu}$ by changing a value of θ.

Artificial field for vibronic state

In the main article, we examine a connection between the Hamiltonian $\mathcal{H}_{\mathrm{eff}} = \mathcal{H}_{\mathrm{exch}} + \mathcal{H}_{\mathrm{JT}}$ and the Heisenberg model $\mathcal{H}_{\mathrm{spin}} = J\sum_{\langle ij\rangle}\boldsymbol{S}_i\cdot\boldsymbol{S}_j$ by introducing the artificial field for the orbital-lattice sector. We introduce the external field which acts on the eigen states $\Phi_{E_{\pm}^{(L)}}$ and $\Phi_{E_{\pm}^{(H)}}$ as

$$\begin{aligned}\mathcal{H}_M = -h_M\Big(&|\Phi_{E_{-}^{(L)}}\rangle\langle\Phi_{E_{-}^{(L)}}| - |\Phi_{E_{+}^{(L)}}\rangle\langle\Phi_{E_{+}^{(L)}}| \\ & -|\Phi_{E_{-}^{(H)}}\rangle\langle\Phi_{E_{-}^{(H)}}| + |\Phi_{E_{+}^{(H)}}\rangle\langle\Phi_{E_{+}^{(H)}}|\Big).\end{aligned} \tag{23}$$

In the Wannier function representation, we have

$$\mathcal{H}_M = -h_M\sum_i \sigma_i^z \otimes F_i, \tag{24}$$

where the 2×2 matrix, σ_i^z, is given for the index μ. The 3×3 matrix is defined by $(F)_{\nu\nu'} = \frac{i}{\sqrt{3}}\sum_l \varepsilon_{l\nu\nu'}$ for the index ν, and is explicitly given as

$$F_i = \frac{1}{\sqrt{3}}\begin{array}{c} \begin{array}{ccc} \Phi_{\mu 0} & \Phi_{\mu 1} & \Phi_{\mu 2} \end{array} \\ \begin{pmatrix} 0 & i & -i \\ -i & 0 & i \\ i & -i & 0 \end{pmatrix} \end{array}. \tag{25}$$

A schematic energy levels under the external field is given in Fig. 6. Double degeneracies in the $E^{(L)}$ and $E^{(H)}$ levels are lifted by applying the virtual field. In the limit of $h_M \to \infty$, the orbital and vibrational degrees of freedom are frozen, and $\mathcal{H}_{\mathrm{eff}} = \mathcal{H}_{\mathrm{exch}} + \mathcal{H}_{\mathrm{DJT}}$ is reduced into the Heisenberg model $\mathcal{H}_{\mathrm{spin}}$ on a honeycomb lattice.

[1] W. A. Harrison, *Electronic Structure and the Properties of Solids, The Physics of the Chemical Bond*, (W. H. Freeman and Company, San francisco, 1980).

[2] Y. Mizuno, *et al.*, Phys. Rev. B **57**, 5326 (1998).

[3] J. S. Koehler and D. M. Dennison, Phys. Rev. **57**, 1006 (1940).

[4] M. C. M. O'Brien, Proc. Roy. Soc. (London) **A281**, 323 (1964).